Open access • Posted Content • DOI:10.1101/2021.03.16.435594

Circular RNA Vaccines against SARS-CoV-2 and Emerging Variants — Source link

Liang Qu, Zongyi Yi, Yong Shen, Yiyuan Xu ...+11 more authors

Institutions: Peking University, Peking Union Medical College

Published on: 16 Mar 2021 - bioRxiv (Cold Spring Harbor Laboratory)

Topics: Circular RNA

Circular RNA Vaccines against SARS-CoV-2 and Emerging Variants

Liang Qu[1]*, Zongyi Yi[1,2]*, Yong Shen[1,2], Yiyuan Xu[1], Zeguang Wu[1], Huixian Tang[1], Xia Xiao[3], Xiaojing Dong[3], Li Guo[3], Ayijiang Yisimayi[4], Yunlong Cao[4], Zhuo Zhou[1], Jianwei Wang[3], Xiaoliang Sunney Xie[4], Wensheng Wei[1]†

[1]Biomedical Pioneering Innovation Center, Beijing Advanced Innovation Center for Genomics, Peking-Tsinghua Center for Life Sciences, Peking University Genome Editing Research Center, State Key Laboratory of Protein and Plant Gene Research, School of Life Sciences, Peking University, Beijing 100871, China. [2]Academy for Advanced Interdisciplinary Studies, Peking University, Beijing 100871, China. [3]NHC Key Laboratory of Systems Biology of Pathogens and Christophe Mérieux Laboratory, Institute of Pathogen Biology, Chinese Academy of Medical Sciences and Peking Union Medical College, Beijing 100730, China; Key Laboratory of Respiratory Disease Pathogenomics, Chinese Academy of Medical Sciences and Peking Union Medical College, Beijing 100730, China. [4]Biomedical Pioneering Innovation Center, Beijing Advanced Innovation Center for Genomics, Peking-Tsinghua Center for Life Sciences, Peking University, Beijing 100871, China.

*These authors contributed equally to this work.

†Email: wswei@pku.edu.cn (W.W.)

Abstract: SARS-CoV-2 has caused a worldwide pandemic. The emerging variants B.1.1.7 in the UK, B.1.351 in South Africa, and P.1 in Brazil have recently spread rapidly, arousing concerns about the efficacy of the current vaccines and antibody therapies. Therefore, there is still a high demand for alternative vaccines with great efficacy, high design flexibility, and fast manufacturing speed. Here, we reported a circular RNA (circRNA) vaccine that encodes the trimeric RBD of SARS-CoV-2 spike protein. Being a circularized RNA molecule, circRNA^{RBD} could be rapidly produced via *in vitro* transcription and is highly stable without nucleotide modification. Lipid-nanoparticle-encapsulated circRNA^{RBD} elicited potent and sustained neutralizing antibodies, as well as Th1-biased T cell responses in mice. Notably, antibodies from mice immunized with circRNA encoding RBD variant (K417N-E484K-501Y) effectively neutralized B.1.351 variant.

Moreover, we developed therapeutic circRNAs, encoding SARS-CoV-2 neutralizing nanobodies or hACE2 decoys, which could effectively neutralize SARS-CoV-2 pseudovirus. Our study suggests that circular RNA holds the potential to become a novel vaccine and therapeutic platform.

Main Text:

Coronavirus disease 2019 (COVID-19) is a serious worldwide public health emergency caused by a novel severe acute respiratory syndrome coronavirus (SARS-CoV-2) (*1, 2*). To date, COVID-19 has resulted in more than one hundred million confirmed cases and over two million confirmed deaths (World Health Organization). Thus, there is an urgent need for the development of safe and effective vaccines against SARS-CoV-2 infection.

SARS-CoV-2, together with Severe Acute Respiratory Syndrome (SARS)-CoV and Middle East Respiratory Syndrome (MERS)-CoV, other two highly pathogenic coronaviruses, belongs to the genus *Betacoronavirus* of the *Coronaviridae* family (*3*). SARS-CoV-2 is a single-strand, positive-sense, enveloped virus, and its virion is composed of an inner capsid formed by 30-kb RNA genome wrapped by the nucleocapsid (N) proteins and a lipid envelope coated with the membrane (M), envelope (E), and trimeric spike (S) proteins (*4*). The S protein of SARS-CoV-2, composed of S1 and S2 subunits, is the major surface protein of the virion. The S protein mediates viral entry into host cells by binding to its receptor, angiotensin-converting enzyme 2 (ACE2), through the receptor-binding domain (RBD) at the C terminus of the S1 subunit. This binding subsequently induces the fusion between the SARS-CoV-2 envelope and the host cell membrane mediated by the S2 subunit, leading to the release of the viral genome into the cytoplasm (*5-8*).

The S protein, S1 subunit, or the RBD antigen of SARS-CoV-2, could induce both B cell and T cell responses, generating highly potent neutralizing antibodies against SARS-CoV-2 (*9-11*). Vaccination is the most promising approach to end COVID-19 pandemic. Traditional vaccine platforms, such as inactivated vaccines, virus-like particle vaccines, and viral vector-based vaccines have been adopted to develop SARS-CoV-2 vaccines (*12-20*). Importantly, the mRNA vaccines against SARS-CoV-2 have been developed at warp speed and urgently approved for use (*21-27*), despite the fact that such strategy had never been applied commercially before (*28*). The mRNA vaccine contains a linear single-strand RNA, consisting of 5' cap, the untranslated region (UTR), antigen-coding region, and 3' polyA tail, which is delivered into bodies via lipid-nano

particle (LNP) encapsulation (*28*). The clinical-scale mRNA vaccines could be manufactured rapidly upon the viral antigen sequence is released (*21*). However, the current mRNA vaccine still has certain limitations due to its inherent instability and suboptimal thermostability after LNP encapsulation for *in vivo* administration (*29-31*), as well as potential immunogenic side effects (*32, 33*).

Circular RNAs (circRNAs) are covalently closed single-stranded RNA transcripts, comprising a large class of non-coding RNAs generated by a non-canonical RNA splicing event called backsplicing in eukaryotic cells (*34-36*). Some viral genomes happen to be circular RNAs, such as hepatitis D virus and plant viroids (*33*). In recent years, thousands of circRNAs have been identified in eukaryotes, including fungi, plants, insects, fish, and mammals via high-throughput RNA sequencing and circRNA-specific bioinformatics (*36*). Unlike linear mRNA, circRNA is highly stable as its covalently closed ring structure protects it from exonuclease-mediated degradation (*36-38*). So far, only a few endogenous circRNAs have been shown to function as protein translation templates (*39-42*). Although circRNA lacks the essential elements for cap-dependent translation, it can be engineered to enable protein translation through internal ribosome entry site (IRES) or the m6A modification incorporated to its 5' UTR region (*43, 44*).

Here, we developed circRNA vaccines against the native SARS-CoV-2 or its emerging variants, which induced robust neutralizing antibodies and strong T cell responses in mice. Moreover, circRNA could be employed to express nanobodies or AEC2 decoys to neutralize the SARS-CoV-2 pseudovirus, manifesting its therapeutics potential to directly blockade such deadly infections.

In Vitro **circRNA production by Group I ribozyme autocatalysis**

We adopted a Group I ribozyme autocatalysis strategy (*43*) to produce circular RNA encoding SARS-CoV-2 RBD antigens (*23*), termed circRNA^{RBD} (Fig. 1A). To enhance the immunogenicity of RBD antigens, we added a signal peptide sequence (SP) to the N-terminus of RBD for its secretory expression (*45-47*). In this construct, the IRES element was placed before the RBD-coding sequence to initiate its translation. The signal peptide sequence of human tissue plasminogen activator (tPA) (*17, 45*) was fused to the N-terminus of RBD to ensure the secretion of antigens, and the trimerization motif of bacteriophage T4 fibritin protein (foldon) (*48*) was fused

to its C terminus, mimicking the natural conformation of SARS-CoV-2 Spike trimers, which have a superior hACE2 binding capacity to the monomeric RBD counterparts (*6, 7, 49*). This IRES-SP-RBD-T4 sequence was then inserted into the cyclization vector (Fig. 1A) to generate the template for *in vitro* transcription (IVT) in order to produce circRNA^{RBD}. The circularization of circRNA^{RBD} was verified (Fig. 1B) by reverse transcription and RT-PCR analysis using specific primers (Fig. 1A).

Owing to this covalently closed circular structure, the circRNA^{RBD} migrated faster in electrophoresis (fig. S1A) and appeared more resistant to exonuclease RNase R than the linear RNAs (fig. S1B). Moreover, the high-performance liquid chromatography (HPLC) purification showed that the RNase R treatment purged significant amount of the linear precursor RNAs, an important step for the production and purification of the circRNA^{RBD} (fig. S1C).

Thermal stable circRNA^{RBD} produces functional SARS-CoV-2 RBD antigens

To test the secretory expression of RBD produced by circRNA^{RBD}, the purified circRNA^{RBD} was transfected into HEK293T cells. We detected ample production of SARS-CoV-2 RBD antigens in the supernatant by Western blot (Fig. 1C). Quantitative ELISA assay showed that the RBD protein reached ~143 ng/mL in the supernatant, 50-fold more than the linear RNA^{RBD} group (Fig. 1D). We further confirmed that circRNA^{RBD} could be expressed in murine NIH3T3 cells (Fig. 1E). Together, these results demonstrated that robust secretory RBD antigens could be produced using circRNA^{RBD} in both human and murine cells.

The inherent stability of circRNA has been reported (*50*), and such a feature would make circRNA an attractive vaccine candidate. To test this, circRNA^{RBD} was stored at room temperature (~25°C) for various days before transfected into HEK293T cells. We found that circRNA^{RBD} could be readily expressed without detectable loss even after two weeks of shelf time (Fig. 1F), highlighting its remarkable thermal stability.

To further verify whether the secreted SARS-CoV-2 RBD antigens produced by circRNA^{RBD} were functional, the supernatants of circRNA^{RBD}-transfected cells were used for competition assay using hACE2-overexpressing HEK293 cells (HEK293T-ACE2) and SARS-CoV-2 pseudovirus harboring an EGFP reporter (*51*). We witnessed that the secreted SARS-CoV-2 RBD antigens

could effectively block SARS-CoV-2 pseudovirus infection (Fig. 1G and fig. S2). Altogether, circRNA^{RBD} showed robust protein expression and high thermal stability, illuminating its potential for vaccination.

SARS-CoV-2 circRNA vaccines elicit sustained humoral immune responses with high-level neutralizing antibodies

With its stability and immunogen-coding capability, we reasoned that circRNA could be developed into a new type of vaccine. We then attempted to assess the immunogenicity of circRNA^{RBD} encapsulated with lipid nanoparticle in BALB/c mice (Fig. 2A). The circRNA^{RBD} encapsulation efficiency was greater than 93%, with an average size of 100 nm in diameter (Fig. 2B). Animals were immunized with LNP-circRNA^{RBD} through intramuscular injection twice, using a dose of 10 μg or 50 μg per mouse at a two-week interval, while empty LNP was used as the placebo (Fig. 2C). The amount of RBD-specific IgG and pseudovirus neutralization activity were evaluated at two or five weeks post LNP-circRNA^{RBD} boost.

High titers of RBD-specific IgG were elicited by circRNA^{RBD} in a dose-dependent manner, ~3×10^4 and ~1×10^6 for each dose and for both 2- and 5-weeks post boost, indicating that circRNA^{RBD} could induce long-lasting antibodies against SARS-CoV-2 RBD (Fig. 2D).

To test the antigen-specific binding capability of IgG from vaccinated animals, we performed a surrogate neutralization assay (*52*). In line with the amount of RBD-specific IgG (Fig. 2D), antibodies elicited by circRNA^{RBD} vaccines showed evident neutralizing capacity in dose-dependent manner, with an NT50 of ~2×10^4 for the dose of 50 μg (Fig. 2, E and F).

We further demonstrated that sera from circRNA^{RBD}-vaccinated mice neutralized SARS-CoV-2 pseudovirus (Fig. 2G), with an NT50 of ~5.6×10^3 in mice immunized with 50 μg of circRNA^{RBD} vaccine. The large amount of RBD-specific IgG, potent RBD antigen neutralization, and sustained SARS-CoV-2 pseudovirus neutralizing capacity suggest that circRNA^{RBD} vaccines did induce a long-lasting humoral immune response in mice.

SARS-CoV-2 circRNA vaccines induce strong T cell immune responses in the spleen

B cells (the source of antibodies), $CD4^+$ T cells, and $CD8^+$ T cells are three pillars of adaptive

148 immunity, and they mediated effector functions that have been associated with the control of
149 SARS-CoV-2 in both non-hospitalized and hospitalized cases of COVID-19 (*53*).

150 To probe $CD4^+$ and $CD8^+$ T cell immune responses in $circRNA^{RBD}$ vaccinated mice (5 weeks
151 post-boost), splenocytes were stimulated with SARS-CoV-2 Spike RBD pooled peptides (Table
152 S1), and cytokine-producing T cells were quantified by intracellular cytokine staining among
153 effector memory T cells (Tem, $CD44^+CD62L^-$) (fig. S3). Stimulated with RBD peptide pools,
154 $CD4^+$ T cells of mice immunized with $circRNA^{RBD}$ vaccines exhibited Th1-biased responses,
155 producing interferon-γ (IFN-γ), tumor necrosis factor (TNF-α), and interleukin-2 (IL-2) (Fig. 3, A
156 and B), but not interleukin-4 (IL-4) (fig. S4), indicating that $circRNA^{RBD}$ vaccines mainly induced
157 the Th1- but not the Th2-biased immune responses. In addition, multiple cytokine-producing $CD8^+$
158 were detected in $circRNA^{RBD}$ vaccinated mice (Fig. 3, C and D). For unknown reasons, 10 μg of
159 $circRNA^{RBD}$ elicited stronger immune responses in both $CD4^+$ and $CD8^+$ effector memory T cells
160 than 50 μg (Fig. 3, A to D), while the latter induced higher potency of neutralizing antibodies in
161 the B cell responses (Fig. 2G).

162 Collectively, these results demonstrated that SARS-CoV-2 $circRNA^{RBD}$ vaccines could induce
163 high level of humoral and cellular immune responses in mice.

164

165 **SARS-CoV-2 $circRNA^{RBD\text{-}501Y.V2}$ vaccines show preferential neutralization activity against**
166 **B.1.351 variant**

167 Next, we evaluated the efficacy of a circRNA vaccine encoding RBD/K417N-E484K-N501Y
168 derived from the B.1.351/501Y.V2 variant, termed as $circRNA^{RBD\text{-}501Y.V2}$ (Fig. 4A). BALB/c mice
169 were immunized with an i.m. injection of the $circRNA^{RBD\text{-}501Y.V2}$ vaccine, followed by a boost at a
170 two-week interval. The immunized mice's sera were collected at 1 and 2 weeks post the boost. The
171 ELISA showed that the RBD-501Y.V2-specific IgG titer reached 7×10^4 at 2 weeks post boost (Fig.
172 4B). The surrogate neutralization assay showed that sera of $circRNA^{RBD\text{-}501Y.V2}$ immunized mice
173 effectively neutralized RBD antigens (Fig. 4C). We then went on to assess the neutralization
174 activity of the sera from mice immunized with $circRNA^{RBD}$ or $circRNA^{RBD\text{-}501Y.V2}$ vaccines against
175 D614G, B.1.1.7/501Y.V1, or B.1.351/501Y.V2 variants. VSV-based pseudovirus neutralization
176 assay revealed that antibodies elicited by $circRNA^{RBD}$ vaccines, which encode the native RBD
177 sequence, effectively neutralized all three viral strains, with the highest activity against the D614G

strain (Fig. 4D). The circRNA$^{RBD\text{-}501Y.V2}$ immunized mouse serum could also neutralize all three pseudoviruses, with the highest neutralization activity against its corresponding variant, 501Y.V2 (Fig. 4E). Collectively, circRNA vaccines-elicited antibodies showed the best neutralization activity against their corresponding variant strains. It's worth noting that both vaccines could neutralize all three strains albeit with variable efficacies. Nevertheless, the multivalent vaccines should have provided better protection for both native SARS-CoV-2 strain and its circulating variants.

Expression of SARS-CoV-2 neutralizing antibodies via circRNA platform

Besides vaccine, circRNA could be re-purposed for therapeutics when used to express some other proteins or peptides, such as enzymes for rare diseases and antibodies for infectious diseases or cancer. Here, we attempted to test the therapeutic potential of circRNAs by expressing the SARS-CoV-2 neutralizing antibodies. It has been reported that SARS-CoV-2 neutralizing nanobodies or hACE2 decoys could inhibit the SARS-CoV-2 infection (*54-56*). This prompted us to leverage the circRNA platform to express SARS-CoV-2 neutralizing nanobodies, including nAB1, nAB1-Tri, nAB2, nAB2-Tri, nAB3, and nAB3-Tri (*54, 55*), together with hACE2 decoys (*56*) (Fig. 5A). Pseudovirus neutralizing assay showed that supernatants of HEK293T cells transfected with circRNA^{nAB} or circRNA$^{hACE2\ decoys}$ could effectively inhibit pseudovirus infection (Fig. 5B). Among those, nAB1-Tri, nAB2, nAB2-Tri, and nAB3-Tri nanobodies produced by circRNAs completely blocked pseudovirus infection.

Discussion

COVID-19 is still a fast-growing global health crisis with circulating SAS-CoV-2 variants evading current vaccines elicited antibodies (*57-59*). This report established a novel approach using circRNA to produce SARS-CoV-2 related interventions, including vaccine, therapeutic nanobodies, and hACE2 decoys.

Several studies have reported that the full-length Spike protein (mRNA-1273 and BNT162b2) (*21, 22, 27*) or RBD-based mRNA vaccines elicit neutralizing antibodies and cellular immune responses (*23-26, 60*). As reported, most effective neutralizing antibodies recognize the RBD

region of S protein (*54, 55, 61-64*) and targeting RBD may induce less amount of non-neutralizing antibodies (*23-26, 60*). Given that RBD trimers were superior in binding hACE2 compared to their monomeric counterparts (*49*), we chose to express RBD trimers as the immunogen.

We highlight this generalizable strategy for designing immunogens. The coding sequence of circular RNA can be quickly adapted to deal with any emerging SARS-CoV-2 variants, such as the recently reported B.1.1.7/501Y.V1, B.1.351/501Y.V2, and P.1 variants (*58, 65, 66*). Moreover, circular RNAs could be quickly generated in large quantities *in vitro*, and they do not require any nucleotide modification, strikingly different from the canonical mRNA vaccines. Interestingly, circular RNA itself could serve as a vaccine adjuvant (*33*), suggesting that circRNA vaccine is likely benefit from its own adjuvant effect.

In this report, circRNA$^{RBD\text{-}501Y.V2}$ immunized mice produced high titers of neutralizing antibodies. Given that K417N-E484K-N501Y mutant in RBD reduces its interactions with certain neutralizing antibodies (*58, 67*), we also demonstrated that neutralizing antibodies produced by mice immunized with circRNA^{RBD} or circRNA$^{RBD\text{-}501Y.V2}$ had preferential neutralizing abilities to their corresponding virus strains.

Multiple candidates for the treatment of COVID-19 have been studied during the pandemic, especially those neutralizing antibodies (*54, 55, 61-64*) and engineered soluble natural receptor for the virus, hACE2 (*68, 69*). circRNA-encoded SARS-CoV-2 neutralizing nanobodies or hACE2 decoy all showed strong neutralizing ability *in vitro*. Given that SARS-CoV-2 variants encoding E484K or N501Y or the K417N-E484K-N501Y evade certain neutralizing antibodies induced by mRNA vaccines (*58, 67*), we anticipated that the effect of circRNA-encoded hACE2 decoy might not be affected by virus mutations.

Owing to their specific properties, circRNAs hold potentials in biomedical applications. Nevertheless, the immunogenicity and the safety of circular RNA vaccines or drugs await further investigations.

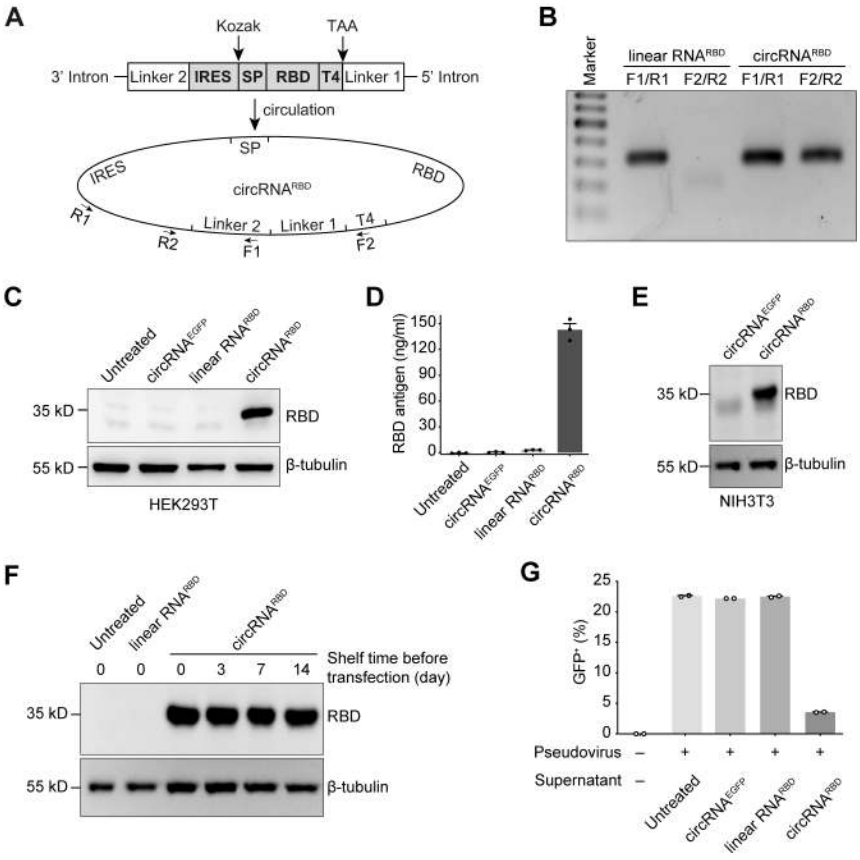

233

234 **Fig. 1. Expression of trimeric SARS-CoV-2 RBD antigens with circular RNAs *in vitro*.** (**A**)
235 Schematic diagram of circRNA^{RBD} circularization by the Group I ribozyme autocatalysis. SP,
236 signal peptide sequence of human tPA protein. T4, the trimerization domain from bacteriophage
237 T4 fibritin protein. RBD, the receptor binding domain of SARS-CoV-2 Spike protein. The arrows
238 indicate the the design of primers for PCR analysis. (**B**) The agarose gel electrophoresis result of
239 the PCR products of linear RNA^{RBD} and circRNA^{RBD}. (**C**) Western Blot analysis showing the
240 expression level of RBD antigens in the supernatant of HEK293T cells transfected with
241 circRNA^{RBD}. The circRNA^{EGFP} and linear RNA^{RBD} were set as controls. (**D**) The quantitative
242 ELISA assay to measure the concentration of RBD antigens in the supernatant. The data in (**B**)
243 was shown as the mean ± S.E.M. (n = 3). (**E**) Western Blot analysis showing the expression level
244 of RBD antigens in the supernatant of mouse NIH3T3 cells transfected with circRNA^{RBD}. The
245 circRNA^{EGFP} was set as controls. (**F**) Western Blot analysis showing the expression level of RBD
246 antigens in the supernatant of HEK293T cells transfected with circRNA^{RBD} for different shelf time
247 (3, 7 or 14 days) at room temperature (~25°C). (**G**) Quantification of the competitive inhibition of
248 SARS-CoV-2 pseudovirus infection (EGFP) by the circRNA^{RBD}-translated RBD antigens. The

circRNA^{EGFP} and linear RNA^{RBD} were set as controls. The data in (**E**) was shown as the mean ± S.E.M. (n = 2).

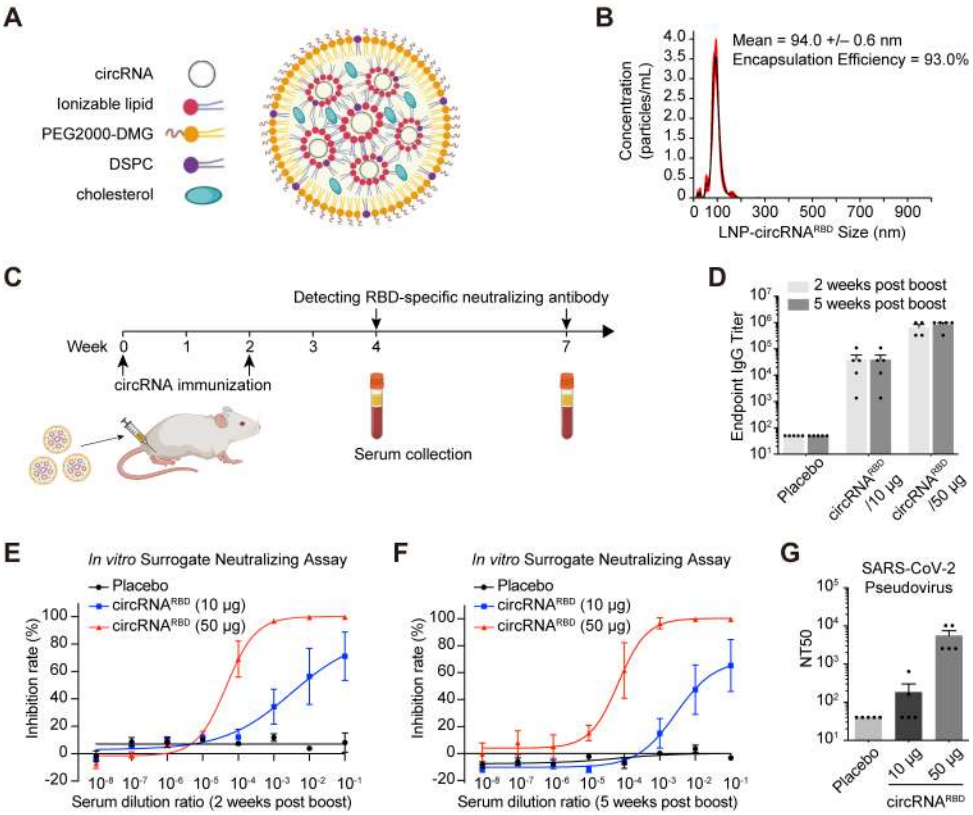

Fig. 2. Humoral immune responses in mice immunized with SARS-CoV-2 circRNA^{RBD} vaccines. (**A**) Schematic representation of LNP-circRNA complex. (**B**) Representative of concentration-size graph of LNP-circRNA^{RBD} measured by dynamic light scattering method. (**C**) Schematic diagram of the LNP-circRNA^{RBD} vaccination process in BALB/c mice and serum collection schedule for specific antibodies analysis. (**D**) Measuring the SARS-CoV-2 specific IgG antibody titer with ELISA. The data were shown as the mean ± S.E.M. (n = 4 or 5). (**E**) Sigmoidal curve diagram of the inhibition rate by sera of immunized mice with surrogate virus neutralization assay. Sera from circRNA^{RBD} (10 μg) and circRNA^{RBD} (50 μg) immunized mice were collected at 2 weeks post the second dose. The data was shown as the mean ± S.E.M. (n = 4). (**F**) Sigmoldal curve diagram of the inhibition rate by sera of immunized mice with surrogate virus neutralization assay. Sera from circRNA^{RBD} (10 μg) and circRNA^{RBD} (50 μg) immunized mice were collected at 5 weeks post boost. The data were shown as the mean ± S.E.M. (n = 5). (**G**) The NT50 was calculated using lentivirus-based SARS-CoV-2 pseudovirus. The data was shown as the mean ± S.E.M. (n = 5).

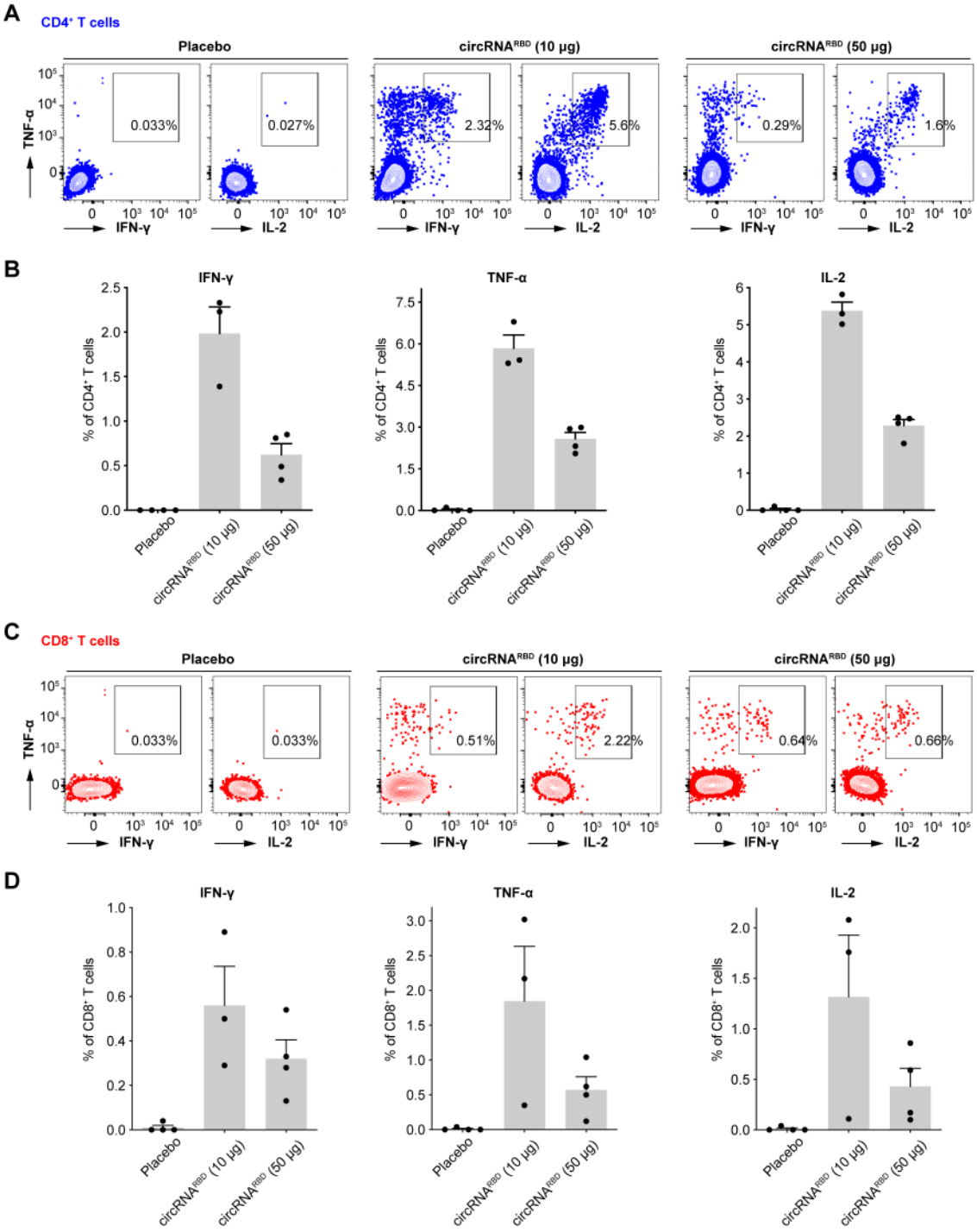

Fig. 3. SARS-CoV-2 specific T cell immune responses in mice immunized with SARS-CoV-2 circRNA^{RBD} vaccines. (**A**) The FACS analysis results showing the percentages of cytokine positive cells evaluated among single and viable CD44^{+}CD62L^{-}CD4^{+} T cells. (**B**) The intracellular staining assay for cytokines (IFN-γ, TNF-α, and IL-2) production among SARS-CoV-2 specific CD4^{+} effector memory T cells (CD44^{+}CD62L^{-}) in splenocytes. (**C**) The FACS analysis results

274 showing the percentages of cytokine positive cells evaluated among single and viable
275 $CD44^+CD62L^-CD8^+$ T. (**D**) The intracellular staining assay for cytokines (IFN-γ, TNF-α, and IL-
276 2) production among SARS-CoV-2 specific $CD8^+$ effector memory T cells ($CD44^+CD62L^-$) in
277 splenocytes. Results were pooled from two independent experiments (**B** and **D**). Data are presented
278 as the mean ± S.E.M. in C and D, n = 3 or 4 for each group. Each symbol represents an individual
279 mouse.

280

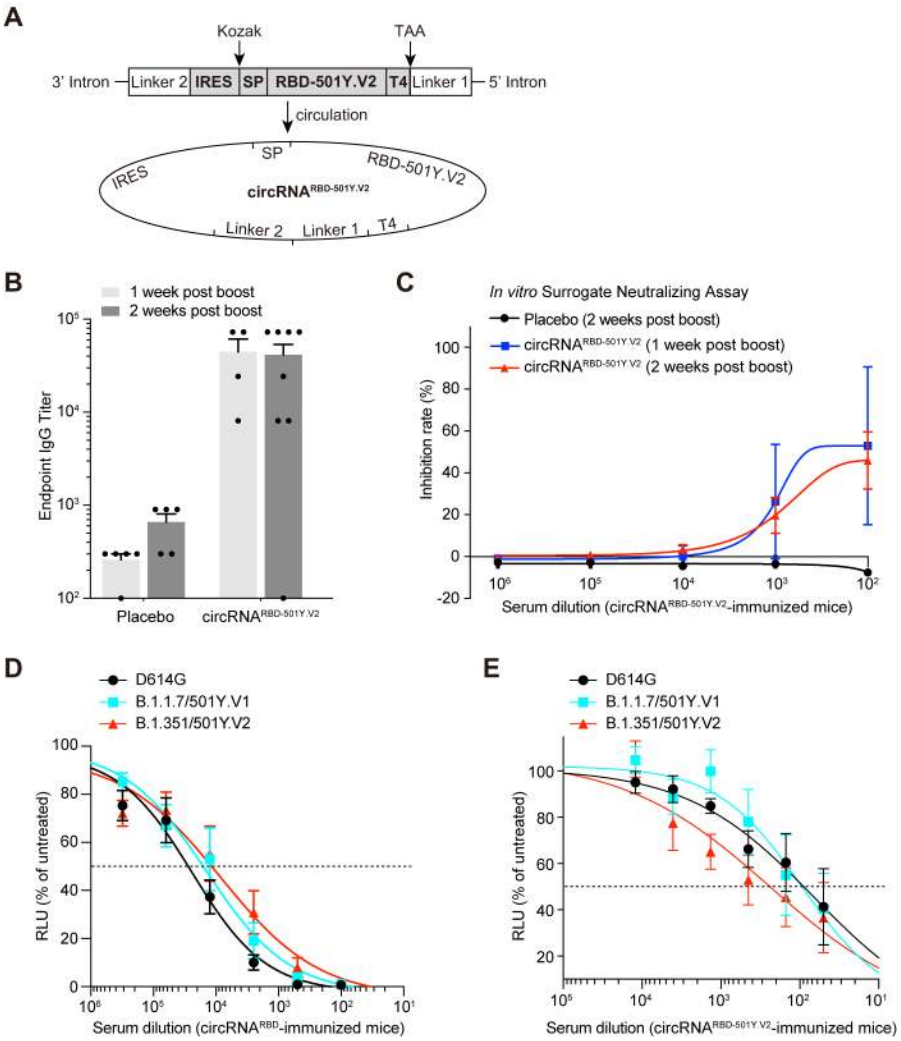

Fig. 4. The susceptibility of SARS-CoV-2 D614G, B.1.1.7 or B.1.351variants to neutralizing antibodies elicited by the circRNA^{RBD} or circRNA$^{RBD\text{-}501Y.V2}$ vaccines in mice. (**A**) Schematic diagram of circRNA$^{RBD\text{-}501Y.V2}$ circularization by the Group I ribozyme autocatalysis. SP, signal peptide sequence of human tPA protein. T4, the trimerization domain from bacteriophage T4 fibritin protein. RBD-501Y.V2, the RBD antigen harboring the K417N-E484K-N501Y mutations in SARS-CoV-2 501Y.V2 variant. (**B**) Measuring the SARS-CoV-2 specific IgG antibody titer with ELISA. The data was shown as the mean ± S.E.M. Each symbol represents an individual mouse. (**C**) Sigmodal curve diagram of the inhibition rate by sera of immunized mice with surrogate virus neutralization assay. Sera from circRNA$^{RBD\text{-}501Y.V2}$ (50 μg) immunized mice were collected at 1 week or 2 weeks post boost. The data were shown as the mean ± S.E.M. (**D**) Neutralization assay of VSV-based D614G, B.1.1.7 or B.1.351 pseudovirus with the serum of mice immunized with circRNA^{RBD} vaccines. The serum samples were collected at 5 weeks post boost. The data were

shown as the mean ± S.E.M. (n = 5). (**E**) Neutralization assay of VSV-based D614G, B.1.1.7 or B.1.351 pseudovirus with the serum of mice immunized with circRNA$^{RBD\text{-}501Y.V2}$ vaccines. The serum samples were collected at 1 week post boost. The data were shown as the mean ± S.E.M. (n = 5).

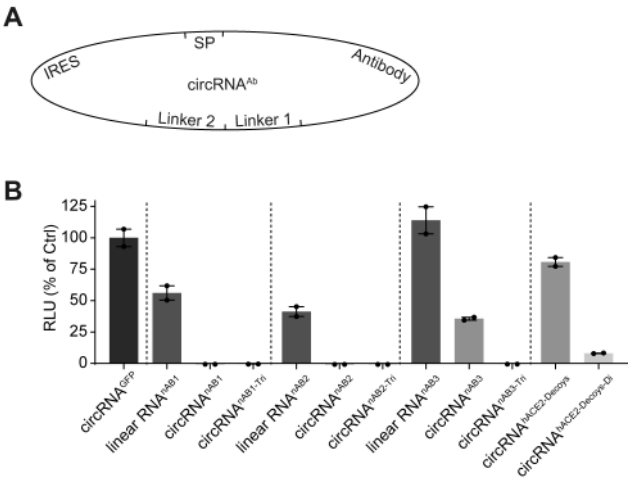

299

300 **Fig. 5. Expression of SARS-CoV-2 neutralizing nanobodies or hACE2 decoys via circRNA**
301 **platform.** (**A**) Schematic diagram of circRNA^{nAB} or circRNA$^{hACE2\ decoys}$ circularization by the
302 Group I ribozyme autocatalysis. (**B**) Lentivirial-based pseudovirus neutralization assay with the
303 supernatant from cells transfected with circRNA encoding neutralizing nanobodies nAB1, nAB1-
304 Tri, nAB2, nAB2-Tri, nAB3 and nAB3-Tri or ACE2 decoys. The luciferase value was normalized
305 to the circRNA^{EGFP} control. The data was shown as the mean ± S.E.M. (n = 2).

306

307

Supplementary Figure Legends

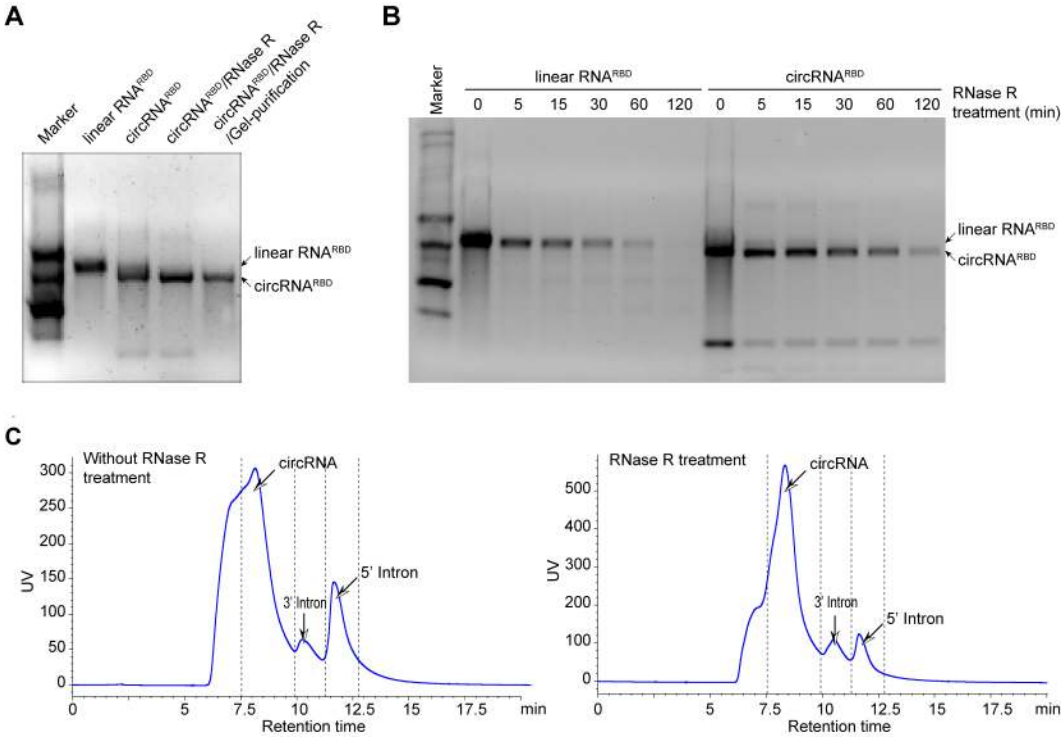

fig S1: Agarose gel electrophoresis and HPLC purification of circRNA^{RBD}. (**A**) The agarose gel electrophoresis result of linear RNA^{RBD} and circRNA^{RBD} with different treatment. (**B**) The agarose gel electrophoresis result of circRNA^{RBD} and linear RNA^{RBD} digested by RNase R with various time from 5 min to 120 min. (**C**) HPLC chromatogram of circRNA^{RBD} without RNase R treatment (left) and circRNA^{RBD} treated by RNase R (right).

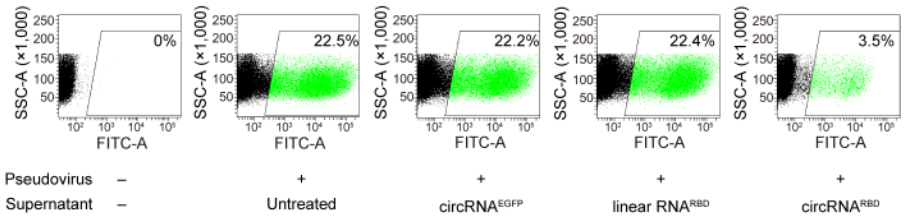

317

318 **fig S2: The FACS chromatogram of the competitive inhibition of SARS-CoV-2 pseudovirus**

319 **infection (harboring EGFP reporter) by the circRNA^{RBD}-translated RBD antigens.**

320

321

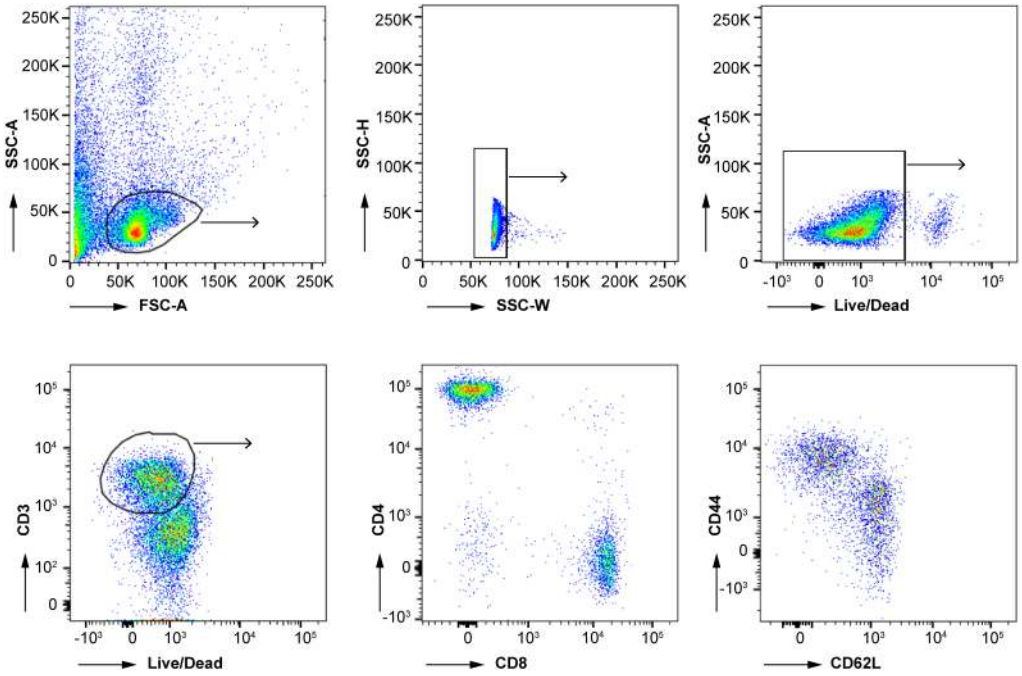

322

323 **fig S3: Flow panel and gating strategy to quantify SARS-CoV-2-RBD-specific T cells in**
324 **mice.** The plots showed the gating strategy of single and viable T cells from spleens. $CD4^+$ or
325 $CD8^+$ T cells were further analyzed with the expression of CD44 and CD62L.

326

327

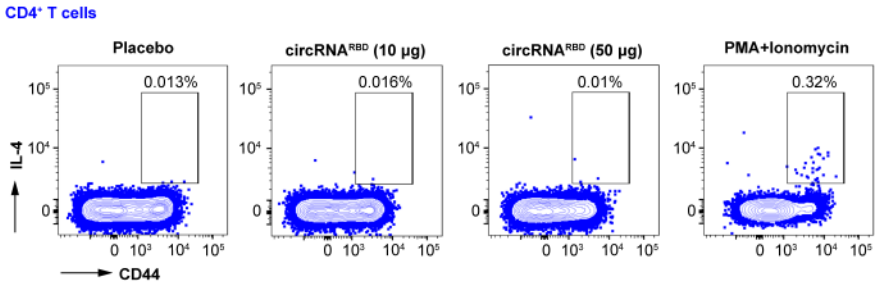

328

329 **fig S4: Identification of IL-4 producing CD4$^+$ T cells in mice immunized with SARS-CoV-2**
330 **circRNA^{RBD} vaccines.** Splenocytes were stimulated with SARS-CoV-2-RBD peptides for 7 hr in
331 the presence of BFA and Monensin. PMA and Ionomycin stimulation were applied as a positive
332 control. Cells were gated on single and viable CD4$^+$ T cells. The plots are representative for two
333 independent experiments with same results.

334

335

Materials and methods

Cell culture

HEK293T and NIH3T3 cell lines were maintained in our laboratory. The HEK293T-hACE2 cell line was ordered from Biodragon Inc. (#BDAA0039, Beijing, China). These mammalian cell lines were cultured in Dulbecco′s Modified Eagle Medium (Corning, 10-013-CV) with 10% fetal bovine serum (FBS) (BI), supplemented with 1% penicillin-streptomycin in 5% CO_2 incubator at 37°C. The Huh-7 cells were maintained in Xie laboratory at Peking University, cultured with the methods previously described (*61*).

circRNA transfection in vitro

For the circRNA transfection in HEK293T or NIH3T3 cells, 3×10^5 cells per well were seeded in 12-well plates. 4 μg of RNase R-treated or HPLC-purified & CIP-treated circRNAs were transfected into the HEK293T or NIH3T3 cells, 24 hr later, using Lipofectamine MessengerMax (Invitrogen, LMRNA003) according to the manufacturer's instructions. 48 hr post transfection, the cell lysis and supernatant were collected for the following detections.

LNP encapsulation of circRNA

The circRNAs were encapsulated with lipid nanoparticle (LNP) through a previously described process (*70*). Briefly, the circRNAs were diluted in the 50 mM citrate buffer (pH 3.0) and the lipids were dissolved and mixed in ethanol at molar ratios of 50:10:38.5:1.5 (MC3-lipid:DSPC:cholesterol:PEG2000-DMG). The lipids mixture was then mixed with the circRNA solution at the volume ratio of 1:3 in the NANOASSEMBLR BENCHTOP (PRECISION, #NIT0046). Then the LNP-circRNA formulations were diluted 40-fold with the 1×PBS buffer (pH 7.2~7.4) and concentrated by ultrafiltration with Amicon® Ultra Centrifugal Filter Unit (Millipore). The concentration and encapsulation rate of circRNAs were measured by the Quant-iT™ RiboGreen™ RNA Assay Kit (Invitrogen™ #R11490). The size of LNP-circRNA particles was measured using dynamic light scattering on a Malvern Zetasizer Nano-ZS 300 (Malvern). Samples were irradiated with red laser (l = 632.8 nm) and scattered light were detected at a

backscattering angle of 173. Results were analyzed to obtain an autocorrelation function using the software (Zetasizer V7.13).

Circulation fragments PCR assay

The circRNA^{RBD} or linear RNA^{RBD} was reverse transcribed into cDNA templates using specific primers with Quantscript RT Kit (KR103, TIANGEN). Then the internal control fragments and junction fragments were PCR amplified from the above cDNA templates with corresponding primers, respectively.

Quantitative determination of SARS-CoV-2 Spike RBD expression in vitro

Quantification of RBD expression in cell culture supernatants was performed with a commercial SARS-CoV-2 Spike RBD Protein ELISA kit (RK04135, ABclonal) according to the manufacturer's instruction. The supernatants were diluted at 1:100 rate. Final concentrations of RBD were calculated basing on the linear standard curve of absorbance at 450 nm, using 630 nm as reference. Briefly, the detection wells were pre-coated with monoclonal antibody specific for Spike RBD protein. After incubation with samples or standards at 37°C for two hours, samples unbound to immobilized antibody would be removed by washing steps. Then the RBD-specific antibodies were added to wells for one-hour incubation at 37°C. After washing, the HRP substrates and stop solution were added and the absorbance at 450 nm were measured using 630 nm as reference.

Mouse vaccination and serum collection

The BALB/c mice were ordered from Beijing Vital River Laboratory Animal Technology Co., Ltd. All mice were bred and kept under SPF (specific pathogen-free) conditions in the Laboratory Animal Center of Peking University. The animal experiments were approved by Peking University Laboratory Animal Center (Beijing), and undertaken in accordance with the National Institute of Health Guide for Care and Use of Laboratory Animals.

For mouse vaccination, groups of 6-8 week-old female BLAB/c mice were intramuscularly immunized with LNP-circRNA^{RBD} (10 μg, N = 5; 50 μg, N = 5), or Placebo (empty LNP, N = 5) in 150 μL using a 1 mL sterile syringe, and 2 weeks later a second dose was immunized to boost the immune responses. The sera of immunized mice were collected at 2 and 5 weeks post the second immunization to detect the SARS-CoV-2-specific IgG titers and neutralizing antibody activity as described below. At 5 weeks post the second immunization, the immunized mice were sacrificed and the splenocytes were isolated for the detection of SARS-CoV-2-specific $CD4^+$ and $CD8^+$ T cell immune responses by Flow cytometry analysis and ELISA as described below.

Antibody titer measurement with ELISA

All the immunized mouse serum samples were heat-inactivated at 56°C for 30 min before use. The SARS-CoV-2-specific IgG antibody titer was measured by ELISA. Briefly, serial 3-fold dilutions (in 1% BSA) of heat-inactivated sera, starting at 1:50, were added to the 96-well plates (100 μL/well; Costar) coated with recombinant SARS-CoV-2 Spike antigens (Sino Biological) and blocked with 1% BSA, and the plates were incubated for at 37°C for 60 min. Then, after three washes with wash buffer, the Horseradish peroxidase HRP-conjugated rabbit anti-mouse IgG (Sigma) diluted in 1% BSA at 1:10,000 ratio (Sigma), was added to the plates and incubated at 37°C for 45 min. Then the plates were washed for 4 times with wash buffer and added with TMB substrates (100 μL/well) followed by incubation for 15-20 min. And then the ELISA stop buffer was added into the plates. Finally, the absorbance (450/630 nm) was measured with Infinite M200 (TECAN). The Endpoint IgG titers were defined as the dilution, which emitted an optical density exceeding 3x background (without serum but secondary antibody was added).

SARS-CoV-2 Surrogate Virus Neutralization Assay

The neutralizing activity of mouse serum samples was detected by SARS-CoV-2 Surrogate Virus Neutralization Test Kit (L00847A, GenScript). Detections were performed according to manufacturer's instruction. Serial 10-fold dilutions of heat-inactivated sera, starting at 1:10, were incubated with HRP-conjugated RBD solutions at 37°C for half an hour, and then the mixtures were added into 96-well plates pre-coated with human ACE2 (hACE2) proteins and incubated for

15 min at 37°C. After washing the TMB substrates and stop solutions were added and the absorbance (450/630 nm) was measured with Infinite M200 (TECAN). The inhibition rates of serum samples were calculated according to the following formula. The half-neutralization titer of serum (NT50) was determined using four-parameter nonlinear regression in Prism 8 (GraphPad).

Inhibition rate = (1- OD value of sample/OD value of negative control) × 100%

Pseudovirus-based neutralization assay

The production of lentivirus-based SARS-CoV-2 pseudovirus and neutralization assay were performed as described previously (*71*). Briefly, the SARS-CoV-2 pseudovirus were produced by co-transfecting plasmids psPAX2 (6 μg), pSpike (6 μg), and pLenti-Luc-GFP (6 μg) into HEK293T cells using X tremeGENE HP DNA Transfection Reagent (Roche) according to the manufacturer's instructions. 48 hr post transfection, the supernatants containing pseudovirus particles were harvested and filtered through a 0.22-μm sterilized membrane for the neutralization assay as described below.

For the determination of NT50 of immunized mouse serum, the HEK293T-hACE2 cells were seeded in 96-well plates (50,000 cells/well) and incubated for approximate 24 hr until reaching over 90% confluent, preparing for pseudovirus infection. The mouse serum was 3-fold diluted, starting at 1:40, and incubated with the SARS-CoV-2 pseudovirus (MOI ≈ 0.05) at 37°C for 60 min. The DMEM medium without serum was used as the negative control group. Then the supernatant of HEK293T-hACE2 cells were removed and the mixer of serum and pseudovirus were added to each well. 36-48 hr later, the luciferase activity, which reflecting the degree of SARS-CoV-2 pseudovirus transfection, was measured using the Nano-Glo Luciferase Assay System (Promega). The 50% neutralization titer (NT50) was defined as the fold-dilution, which emitted an exceeding 50% inhibition of pseudovirus infection in comparison with the control group.

The neutralization assay of VSV-based pseudovirus of SARS-CoV-2 and variants was performed as described previously (*61, 62*). Briefly, serum was diluted at 1:100 with 5 additional serial 5-fold dilution, and incubated with the same volume of pseudovirus with a $TCID_{50}$ of 1.3×10^4 for 60 min at 37°C. 20,000 Huh-7 cells/well were cultured with mixture at 37°C for 24 h. Luciferase activity was measured using the britelite plus Reporter Gene Assay System (PerkinElmer).

Relative luciferase units (RLU) were normalized to untreated groups, and analyzed by four-parameter nonlinear regression in Prism (GraphPad).

For the neutralization assay of circRNA^{nAB} or circRNA$^{ACE2\ decoys}$, the HEK293T-hACE2 cells were seeded in 96-well plates (50,000 cells/well) and incubated for approximate 24 hr until reaching over 90% confluent. The pseudovirus were pre-incubated with the supernatant of the circRNA^{nAB} or circRNA$^{ACE2\ decoys}$ transfected cells at 37°C for 60 min, and then added to cells in the 96-well plates. Media were changed at 24 hr after transduction. All cells were collected at 48 hr after transduction. Luciferase activity was measured using the Nano-Glo Luciferase Assay System (Promega). The relative luminescence units were normalized to cells infected with supernatant of cell transfected with the circRNA^{EGFP}.

T cell flow cytometry analysis

The Splenocytes from each immunized mouse were cultured in R10 media (RPMI 1640 supplemented with 1% Pen-Strep antibiotic, 10% HI-FBS), stimulated with RBD peptide pools (Table S1) (Sangon Biotech) for 7 hr at 37°C with protein transport inhibitor cocktail (added 3 hr later). Peptide pools were used at a final concentration of 2 μg/mL for each peptide. Cells from each group were pooled for stimulation with cell stimulation cocktail (PMA/Ionomycin) as a positive control. Following stimulation, cells were washed with PBS prior to staining with LIVE/DEAD for 20 min at room temperature. Cells were then washed in stain buffer (PBS supplemented with 2.5% FBS) and suspended in Fc Block for 5 min at RT prior to staining with a surface stain of following antibodies: CD3 (Invitrogen, 45-0031-82)/CD4 (BD, 562285)/CD8 (BD, 553035)/CD69 (BD, 557392)/CD44 (BD, 563058)/CD62L (BD, 560507). After 20 min, cells were washed with stain buffer, and then fixed and permeabilized using the BD Cytoperm fixation/permeabilization solution kit according to manufacturer instructions. Cells were washed in perm/wash solution, followed by intracellular staining (30 min, RT) using a cocktail of the following antibodies: IFN-γ (BD, 557998)/IL-2 (BD, 560547)/IL-4 (BD, 554435)/TNF-a (BD, 557644). Finally, cells were washed in perm/wash solution and suspended in stain buffer. Samples were washed and acquired on a LSRFortessa (BD Biosciences). Analysis was performed using FlowJo software.

Expression of neutralizing nanobodies or ACE2 decoys by circular RNAs

HEK293T cells were transfected with circular RNA in transfection reagent. Circular RNA encoding secretary nanobodies or hACE2 decoys were purified after GTP treatment for cyclization. In brief, HEK293T cells were seeded in 12-well plates. After 24 h, cells were transfected with circRNA (4 μg per well) and continuously added fresh medium to a final volume of about 1 ml. Supernatants were harvested at 48 hr post transfection and centrifuged to remove cells.

REFERENCES

1. F. Wu *et al.*, A new coronavirus associated with human respiratory disease in China. *Nature* **579**, 265-269 (2020).
2. P. Zhou *et al.*, A pneumonia outbreak associated with a new coronavirus of probable bat origin. *Nature* **579**, 270-273 (2020).
3. P. V'Kovski, A. Kratzel, S. Steiner, H. Stalder, V. Thiel, Coronavirus biology and replication: implications for SARS-CoV-2. *Nat Rev Microbiol* **19**, 155-170 (2021).
4. D. Kim *et al.*, The Architecture of SARS-CoV-2 Transcriptome. *Cell* **181**, 914-921 e910 (2020).
5. M. Hoffmann *et al.*, SARS-CoV-2 Cell Entry Depends on ACE2 and TMPRSS2 and Is Blocked by a Clinically Proven Protease Inhibitor. *Cell* **181**, 271-280 e278 (2020).
6. R. Yan *et al.*, Structural basis for the recognition of SARS-CoV-2 by full-length human ACE2. *Science* **367**, 1444-1448 (2020).
7. D. Wrapp *et al.*, Cryo-EM structure of the 2019-nCoV spike in the prefusion conformation. *Science* **367**, 1260-1263 (2020).
8. J. Shang *et al.*, Cell entry mechanisms of SARS-CoV-2. *Proc Natl Acad Sci U S A* **117**, 11727-11734 (2020).
9. A. C. Walls *et al.*, Structure, Function, and Antigenicity of the SARS-CoV-2 Spike Glycoprotein. *Cell* **181**, 281-292 e286 (2020).
10. C. L. Hsieh *et al.*, Structure-based design of prefusion-stabilized SARS-CoV-2 spikes. *Science* **369**, 1501-1505 (2020).
11. S. Bangaru *et al.*, Structural analysis of full-length SARS-CoV-2 spike protein from an advanced vaccine candidate. *Science* **370**, 1089-1094 (2020).
12. F. Krammer, SARS-CoV-2 vaccines in development. *Nature* **586**, 516-527 (2020).
13. A. Mullard, COVID-19 vaccine development pipeline gears up. *Lancet* **395**, 1751-1752 (2020).
14. Q. Gao *et al.*, Development of an inactivated vaccine candidate for SARS-CoV-2. *Science* **369**, 77-81 (2020).

15. N. van Doremalen *et al.*, ChAdOx1 nCoV-19 vaccine prevents SARS-CoV-2 pneumonia in rhesus macaques. *Nature* **586**, 578-582 (2020).

16. L. Sanchez-Felipe *et al.*, A single-dose live-attenuated YF17D-vectored SARS-CoV-2 vaccine candidate. *Nature* **590**, 320-325 (2021).

17. F. C. Zhu *et al.*, Safety, tolerability, and immunogenicity of a recombinant adenovirus type-5 vectored COVID-19 vaccine: a dose-escalation, open-label, non-randomised, first-in-human trial. *Lancet* **395**, 1845-1854 (2020).

18. J. Yang *et al.*, A vaccine targeting the RBD of the S protein of SARS-CoV-2 induces protective immunity. *Nature* **586**, 572-577 (2020).

19. L. Dai *et al.*, A Universal Design of Betacoronavirus Vaccines against COVID-19, MERS, and SARS. *Cell* **182**, 722-733 e711 (2020).

20. J. Yu *et al.*, DNA vaccine protection against SARS-CoV-2 in rhesus macaques. *Science* **369**, 806-811 (2020).

21. K. S. Corbett *et al.*, SARS-CoV-2 mRNA vaccine design enabled by prototype pathogen preparedness. *Nature* **586**, 567-571 (2020).

22. K. S. Corbett *et al.*, Evaluation of the mRNA-1273 Vaccine against SARS-CoV-2 in Nonhuman Primates. *The New England journal of medicine* **383**, 1544-1555 (2020).

23. N. N. Zhang *et al.*, A Thermostable mRNA Vaccine against COVID-19. *Cell* **182**, 1271-1283 e1216 (2020).

24. D. Laczko *et al.*, A Single Immunization with Nucleoside-Modified mRNA Vaccines Elicits Strong Cellular and Humoral Immune Responses against SARS-CoV-2 in Mice. *Immunity* **53**, 724-732 e727 (2020).

25. Q. Huang *et al.*, A single-dose mRNA vaccine provides a long-term protection for hACE2 transgenic mice from SARS-CoV-2. *Nature communications* **12**, 776 (2021).

26. U. Sahin *et al.*, COVID-19 vaccine BNT162b1 elicits human antibody and TH1 T cell responses. *Nature* **586**, 594-599 (2020).

27. A. B. Vogel *et al.*, BNT162b vaccines protect rhesus macaques from SARS-CoV-2. *Nature*, (2021).

28. N. Pardi, M. J. Hogan, F. W. Porter, D. Weissman, mRNA vaccines - a new era in vaccinology. *Nat Rev Drug Discov* **17**, 261-279 (2018).

29. N. A. C. Jackson, K. E. Kester, D. Casimiro, S. Gurunathan, F. DeRosa, The promise of mRNA vaccines: a biotech and industrial perspective. *NPJ Vaccines* **5**, 11 (2020).

30. M. Durymanov, J. Reineke, Non-viral Delivery of Nucleic Acids: Insight Into Mechanisms of Overcoming Intracellular Barriers. *Front Pharmacol* **9**, 971 (2018).

31. O. S. Fenton *et al.*, Bioinspired Alkenyl Amino Alcohol Ionizable Lipid Materials for Highly Potent In Vivo mRNA Delivery. *Adv Mater* **28**, 2939-2943 (2016).

32. R. A. Wesselhoeft *et al.*, RNA Circularization Diminishes Immunogenicity and Can Extend Translation Duration In Vivo. *Mol Cell* **74**, 508-520 e504 (2019).

33. Y. G. Chen *et al.*, N6-Methyladenosine Modification Controls Circular RNA Immunity. *Mol Cell* **76**, 96-109 e109 (2019).

34. X. O. Zhang *et al.*, Complementary sequence-mediated exon circularization. *Cell* **159**, 134-147 (2014).

35. L. L. Chen, The biogenesis and emerging roles of circular RNAs. *Nat Rev Mol Cell Biol* **17**, 205-211 (2016).

36. L. S. Kristensen *et al.*, The biogenesis, biology and characterization of circular RNAs. *Nat Rev Genet* **20**, 675-691 (2019).

37. S. Memczak *et al.*, Circular RNAs are a large class of animal RNAs with regulatory potency. *Nature* **495**, 333-338 (2013).

38. Y. Enuka *et al.*, Circular RNAs are long-lived and display only minimal early alterations in response to a growth factor. *Nucleic Acids Res* **44**, 1370-1383 (2016).

39. I. Legnini *et al.*, Circ-ZNF609 Is a Circular RNA that Can Be Translated and Functions in Myogenesis. *Mol Cell* **66**, 22-37 e29 (2017).

40. M. Zhang *et al.*, A novel protein encoded by the circular form of the SHPRH gene suppresses glioma tumorigenesis. *Oncogene* **37**, 1805-1814 (2018).

41. M. Zhang *et al.*, A peptide encoded by circular form of LINC-PINT suppresses oncogenic transcriptional elongation in glioblastoma. *Nat Commun* **9**, 4475 (2018).

42. X. Gao *et al.*, Circular RNA-encoded oncogenic E-cadherin variant promotes glioblastoma tumorigenicity through activation of EGFR-STAT3 signalling. *Nat Cell Biol*, (2021).

43. R. A. Wesselhoeft, P. S. Kowalski, D. G. Anderson, Engineering circular RNA for potent and stable translation in eukaryotic cells. *Nat Commun* **9**, 2629 (2018).

44. Y. Yang *et al.*, Extensive translation of circular RNAs driven by N(6)-methyladenosine. *Cell Res* **27**, 626-641 (2017).

45. Y. Kou *et al.*, Tissue plasminogen activator (tPA) signal sequence enhances immunogenicity of MVA-based vaccine against tuberculosis. *Immunol Lett* **190**, 51-57 (2017).

46. J. M. Richner *et al.*, Modified mRNA Vaccines Protect against Zika Virus Infection. *Cell* **169**, 176 (2017).

47. N. Pardi *et al.*, Zika virus protection by a single low-dose nucleoside-modified mRNA vaccination. *Nature* **543**, 248-251 (2017).

48. K. Papanikolopoulou, M. J. van Raaij, A. Mitraki, Creation of hybrid nanorods from sequences of natural trimeric fibrous proteins using the fibritin trimerization motif. *Methods Mol Biol* **474**, 15-33 (2008).

49. K. M. Bouwman *et al.*, Multimerization- and glycosylation-dependent receptor binding of SARS-CoV-2 spike proteins. *PLoS Pathog* **17**, e1009282 (2021).

50. J. W. Fischer, A. K. Leung, CircRNAs: a regulator of cellular stress. *Crit Rev Biochem Mol Biol* **52**, 220-233 (2017).

51. X. Ou *et al.*, Characterization of spike glycoprotein of SARS-CoV-2 on virus entry and its immune cross-reactivity with SARS-CoV. *Nature communications* **11**, 1620 (2020).

52. C. W. Tan *et al.*, A SARS-CoV-2 surrogate virus neutralization test based on antibody-mediated blockage of ACE2-spike protein-protein interaction. *Nat Biotechnol* **38**, 1073-1078 (2020).

53. A. Sette, S. Crotty, Adaptive immunity to SARS-CoV-2 and COVID-19. *Cell* **184**, 861-880 (2021).

54. Y. Xiang *et al.*, Versatile and multivalent nanobodies efficiently neutralize SARS-CoV-2. *Science* **370**, 1479-1484 (2020).

55. M. Schoof *et al.*, An ultrapotent synthetic nanobody neutralizes SARS-CoV-2 by stabilizing inactive Spike. *Science* **370**, 1473-1479 (2020).

56. T. W. Linsky *et al.*, De novo design of potent and resilient hACE2 decoys to neutralize SARS-CoV-2. *Science* **370**, 1208-1214 (2020).

57. A. Muik *et al.*, Neutralization of SARS-CoV-2 lineage B.1.1.7 pseudovirus by BNT162b2 vaccine-elicited human sera. *Science*, (2021).

58. Z. Wang *et al.*, mRNA vaccine-elicited antibodies to SARS-CoV-2 and circulating variants. *Nature*, (2021).

59. P. Wang *et al.*, Antibody Resistance of SARS-CoV-2 Variants B.1.351 and B.1.1.7. *Nature*, (2021).

60. W. Tai *et al.*, A novel receptor-binding domain (RBD)-based mRNA vaccine against SARS-CoV-2. *Cell Res* **30**, 932-935 (2020).

61. Y. Cao *et al.*, Potent Neutralizing Antibodies against SARS-CoV-2 Identified by High-Throughput Single-Cell Sequencing of Convalescent Patients' B Cells. *Cell* **182**, 73-84 e16 (2020).

62. S. Du *et al.*, Structurally Resolved SARS-CoV-2 Antibody Shows High Efficacy in Severely Infected Hamsters and Provides a Potent Cocktail Pairing Strategy. *Cell* **183**, 1013-1023 e1013 (2020).

63. C. O. Barnes *et al.*, SARS-CoV-2 neutralizing antibody structures inform therapeutic strategies. *Nature* **588**, 682-687 (2020).

64. P. A. Koenig *et al.*, Structure-guided multivalent nanobodies block SARS-CoV-2 infection and suppress mutational escape. *Science* **371**, (2021).

65. N. G. Davies *et al.*, Increased hazard of death in community-tested cases of SARS-CoV-2 Variant of Concern 202012/01. *medRxiv*, (2021).

66. A. S. Lauring, E. B. Hodcroft, Genetic Variants of SARS-CoV-2-What Do They Mean? *JAMA* **325**, 529-531 (2021).

67. C. K. Wibmer *et al.*, SARS-CoV-2 501Y.V2 escapes neutralization by South African COVID-19 donor plasma. *Nat Med*, (2021).

68. K. K. Chan *et al.*, Engineering human ACE2 to optimize binding to the spike protein of SARS coronavirus 2. *Science* **369**, 1261-1265 (2020).

69. A. Glasgow *et al.*, Engineered ACE2 receptor traps potently neutralize SARS-CoV-2. *Proc Natl Acad Sci U S A* **117**, 28046-28055 (2020).

70. L. M. Ickenstein, P. Garidel, Lipid-based nanoparticle formulations for small molecules and RNA drugs. *Expert Opin Drug Deliv* **16**, 1205-1226 (2019).

71. D. Pinto *et al.*, Cross-neutralization of SARS-CoV-2 by a human monoclonal SARS-CoV antibody. *Nature* **583**, 290-295 (2020).

ACKNOWLEDGEMENTS

We acknowledge C. Dong and X. Wang (Tsinghua University) for providing fluorescent-conjugated antibodies. We thank J. Xiao (Peking University) for providing purified SARS-CoV-2 Spike proteins. We thank J. Yan (Institute of Microbiology, Chinese Academy of Sciences) for providing RBD peptide pools. We thank the Laboratory Animal Centre of Peking University for the feeding of mice. We thank the HPLC Core at the National Center for Protein Sciences at Peking University (Beijing), particularly H. Li and G. Li for technical help. We thank the flow cytometry Core at the National Center for Protein Sciences at Peking University (Beijing), particularly H. Lv, Y. Guo, H. Yang, F. Wang for technical help.

Funding:

This project was supported by funds from National Key R&D Program of China (2020YFA0707800 to W.W., 2020YFA0707600 to Z.Z.); Beijing Municipal Science & Technology Commission (Z181100001318009); the National Science Foundation of China (31930016); Beijing Advanced Innovation Center for Genomics at Peking University and the Peking-Tsinghua Center for Life Sciences (to W.W.); the National Science Foundation of China (31870893); the National Major Science & Technology Project for Control and Prevention of Major Infectious Diseases in China (2018ZX10301401 to Z.Z.) and the Fellowship of China National Postdoctoral Program for Innovative Talents (BX20200010, to L.Q.).

Author Contributions:

W.W. conceived and supervised this project. W.W., L.Q. and Z.Y. designed the experiments. L.Q., Z.Y., Y.S., Y.X., Z.W., H.T., A.Y., and X.X. performed the experiments with the help from Z.Z., Y.C., J.W., and X.S.X.. L.Q., Z.Y. and W.W. wrote the manuscript with the help of all other authors.